Energy Conversion and Management 232 (2021) 113795

Contents lists available at ScienceDirect

Energy Conversion and Management

journal homepage: www.elsevier.com/locate/enconman

Energy management of heavy-duty fuel cell vehicles in real-world driving scenarios: Robust design of strategies to maximize the hydrogen economy and system lifetime

Alessandro Ferrara [a,*], Stefan Jakubek [a], Christoph Hametner [b]

[a] Institute of Mechanics and Mechatronics, Division of Process Control and Automation, TU Wien, Getreidemarkt 9/E325, 1060 Vienna, Austria
[b] Christian Doppler Laboratory for Innovative Control and Monitoring of Automotive Powertrain Systems, TU Wien, Getreidemarkt 9/E325, 1060 Vienna, Austria

ARTICLE INFO

Keywords:
Energy management
Power-split
Fuel cell electric vehicles
Heavy-duty electric vehicles
Fuel cells
Fuel cell trucks

ABSTRACT

Energy management is a critical issue for the advancement of fuel cell vehicles because it significantly influences their hydrogen economy and lifetime. This paper offers a comprehensive investigation of the energy management of heavy-duty fuel cell vehicles for road freight transportation. An important and unique contribution of this study is the development of an extensive and realistic representation of the vehicle operation, which includes 1750 hours of real-world driving data and variable truck loading conditions. This framework is used to analyze the potential benefits and drawbacks of heuristic, optimal, and predictive energy management strategies to maximize the hydrogen economy and system lifetime of fuel cell vehicles for road freight transportation. In particular, the statistical evaluation of the effectiveness and robustness of the simulation results proves that it is necessary to consider numerous and realistic driving scenarios to validate energy management strategies and obtain a robust design. This paper shows that the hydrogen economy can be maximized as an individual target using the available driving information, achieving a negligible deviation from the theoretical limit. Furthermore, this study establishes that heuristic and optimal strategies can significantly reduce fuel cell transients to improve the system lifetime while retaining high hydrogen economies. Finally, this investigation reveals the potential benefits of predictive energy management strategies for the multi-objective optimization of the hydrogen economy and system lifetime.

1. Introduction

Road freight transportation is a challenging task for the decarbonization of the transport sector. Heavy-duty vehicles represent a small share of the total vehicle population (for example, less than 5% in the U. S. [1]). However, due to the heavy loads, road freight transportation accounts for one-third of global energy demand and greenhouse gas emissions in the transport sector. This already high burden can worsen in the near future because the freight activity is expected to be more than double by 2050 due to the ever-growing energy demand and the development of emerging countries [2].

Battery electric vehicles and fuel cell electric vehicles can significantly contribute to the global mitigation of greenhouse gases and pollutant emissions. Many commercial models are already available on the market of passenger cars for both categories, showing promising results in terms of range, performance, and driving comfort. However, thanks to higher energy density and fast refueling, fuel cell systems seem more appealing than batteries for heavy-duty vehicles (HDVs), which have higher power and range requirements [1,3,4] than passenger cars. The life-cycle analysis in [1] shows that fuel cell HDVs retain well-to-wheel improvements in energy use and emissions compared to conventional vehicles. Kast et al. [5] segment the HDVs market by weight class and vocation to identify the best-suited applications for fuel cell technology. The analysis suggests that most vehicles have sufficient space for hydrogen storage tanks under the side rails, behind the cab, and under the chassis, to cover their daily operation range. In the largest segment, i.e. class 8 tractor-trailers, 50% of the units have a range lower than 200 km and 90% lower than 880 km.

Three main barriers prevent the commercialization of heavy-duty fuel cell vehicles: high costs, low lifetime, and missing hydrogen refueling infrastructure. Hopefully, technological progress and economies of scale will reduce manufacturing and hydrogen production costs and

* Corresponding author.
E-mail address: alessandro.ferrara@tuwien.ac.at (A. Ferrara).

https://doi.org/10.1016/j.enconman.2020.113795
Received 25 September 2020; Accepted 23 December 2020
Available online 6 February 2021

build up the refueling infrastructure. Additionally, the development of suitable control strategies for vehicle operation is essential to increase the hydrogen economy and system lifetime.

Fuel cell electric vehicles (FCEVs) include battery systems to cope with the fast and frequent load changes typical of vehicle applications. However, the inclusion of ultracapacitor systems is also under investigation to improve performance, efficiency, and lifetime. In general, vehicles with multiple power sources are referred to as *hybrid* and their control is hierarchically divided into levels. First, a supervisory controller performs the load distribution to the multiple power sources. Then, low-level controllers act on the different power sources to follow the set-points imposed by the higher level. For example, a fuel cell controller regulates reactant flows, humidification, and cooling, to supply the power required for the vehicle's propulsion.

The power-split task is usually referred to as *energy management*, and it represents a challenging aspect of the control of hybrid vehicles because it usually has multiple and contrasting objectives. In fuel cell electric vehicles, energy management strategies must be designed to maximize the hydrogen economy, the system lifetime, and sustain the battery charge. In particular, the limited lifetime of fuel cell systems represents the main restriction for the durability of fuel cell vehicles. Here, the degradation is accelerated by frequent start-up/shut-down cycles, dynamic loads, low and high power operation [6–9]. Appendix A provides further details on fuel cell degradation phenomena.

The goal of energy management strategies is to limit the occurrence of detrimental conditions to increase system lifetime without hindering the hydrogen economy. In this work, three key targets are identified to mitigate fuel cell degradation: avoiding shut-down during a single driving cycle, avoiding low-power operation, and reducing transients. The first two targets can be achieved through the idle operation of the fuel cell system. In other words, the fuel cell power can be constrained to a minimum value to avoid shut-downs and low-power operations. Therefore, reducing fuel cell transients remains the only active target to mitigate degradation. Here, avoiding high-power operation is not considered a mitigation target because energy management strategies inherently avoid high power operation due to the lower system efficiency. Moreover, the resulting degradation can be avoided through a proper design of fuel cell controllers.

Energy management strategies (EMSs) are typically classified in *heuristic* or *optimal*. Heuristic strategies are designed using engineering intuition and experience to execute the power split following maps or sets of rules. Optimal strategies involve the minimization of a certain cost function. These strategies derive from optimal control theory and use mathematical optimization methods like dynamic programming, Pontryagin's minimum principle, and nonlinear programming [10]. Energy management strategies can also be classified as *online* or *offline*, depending on whether or not they can be practically implemented in real vehicles. In particular, offline strategies can find the optimal solution to the energy management problem using the complete knowledge of driving cycles. This assumption is not suitable for real vehicles, where only current or past driving information is available. Nevertheless, offline strategies are often adopted to provide useful benchmarks for the design of online ones.

In the last years, academic and industry researchers increasingly focused on energy management because of its importance for advancing and commercializing FCEVs. In preparation for the present work, the available literature has been thoroughly analyzed to identify topics that are yet unexplored or poorly addressed. In particular, the three following issues converge to define the scope of the present work.

- There is a lack of investigations related to heavy-duty fuel cell vehicles for road freight transportation, although this segment has the potential to represent the best sector for the commercialization of FCEVs. Our previous work [11] represents the only related study in the literature, to the authors' knowledge. However, that work mainly focuses on proposing an advanced predictive energy management concept without comparing it to other methods. Therefore, it is not yet clear what kind of strategies are best suited for road freight applications.
- The energy management strategies are usually designed considering a small number of driving cycles. Therefore, there is no guarantee that the strategies are robust and retain their effectiveness when used in unknown driving conditions. The work detailed in [12] is the only one that considers a large number of cycles and offers a statistical evaluation of the results.
- Most works consider standard driving cycles used in the past to assess the emission levels of conventional vehicles. However, these cycles are outdated and usually portray an unrealistic vehicle operation (e.g., NEDC). On the contrary, the design of EMSs should consider real-world driving cycles that are coherent with the class of the vehicle under investigation. Moreover, it should also be mentioned that the elevation of the road is usually neglected, but that this assumption is not reasonable for heavy-duty vehicles due to their significant mass.

Table 1 categorizes some relevant works available in the literature of EMSs for fuel cell/battery vehicles. The categories are vehicle class, the number of strategies investigated, consideration of system lifetime as a target, and the number of driving cycles analyzed. The main features of each work listed in the table are summarized as follows. In particular, Ravey et al. [13] propose an energy management strategy based on fuzzy logic and use a genetic algorithm for its optimal tuning. This approach highlights the potential of optimized rule-based strategies. Ettihir et al. [14] propose an online strategy based on Pontryagin's minimum principle, using a PI controller to regulate the co-state value and keep the battery state of charge in a feasible region. The strategy is adaptive to degradation, thanks to the online estimation of fuel cell characteristics. Fletcher et al. [15] use stochastic dynamic programming to create a multi-dimensional lookup table that can be used for the on-board applications. Targets to limit fuel cell degradation are identified, and lifetime improvements and expectations are analyzed quantitatively. Kemper et al. [12] compare three well-known strategies in terms of hydrogen consumption. The evaluation is meaningful because it considers 60 real-world driving cycles. The correlation between hydrogen consumption and driving characteristics is analyzed by grouping the cycles into 6 clusters. Zhou et al. [16] compare different extremum seeking methods schemes. These strategies are online adaptive optimization algorithms capable of maintaining fuel cell operation in high-efficiency regions. Song et al. [17] evaluate the impact of two simple strategies on the durability of fuel cell key components, applying the heuristic degradation model proposed in [9]. Li et al. [18] propose a model predictive control strategy based on Pontryagin's minimum

Table 1
Summary of the relevant literature on fuel cell/battery vehicles.

Ref.	Vehicle class/weight	No. of EMS	Lifetime	No. of driving cycles
[13]	LD	2	No	1
[14]	LD	1	Yes	1
[15]	LD	2	Yes & No	*10
[12]	LD	3	No	*60
[16]	LD	4	Yes & No	2
[17]	LD	2	Yes & No	3
[18]	LD	3	Yes	7
[11]	HD/ 40t	2	Yes & No	*1
[19]	HD/ 16t	2	Yes & No	4
[20]	HD/ 8t	2	Yes	1
[21]	HD/ 20t	1	Yes	1
[22]	HD/ 13t	1	Yes	3
[23]	HD/ 18t	4	Yes	4
This work	HD/ 14-40t	6	Yes & No	*544

LD: light-duty. HD: heavy-duty. *Real-world driving cycles.

principle. The co-state is selected considering speed predictions to keep the battery state of charge close to a reference value. The speed prediction system is based on an improved Markov chain. Ferrara et al. [11] propose a model predictive control concept for the energy management of a 40-tonnes fuel cell truck. The trade-off between hydrogen consumption and system lifetime is investigated using Pontryagin's minimum principle as a benchmark strategy. Simmons et al. [19] define a strategy based on an auto-regressive moving average model. The strategy is tuned using as a benchmark the results deriving from Pontryagin's minimum principle. Geng et al. [20] propose a strategy based on fuzzy logic for a heavy-duty vehicle. Guo et al. [21] develop a model predictive control framework for integrating speed planning (i.e., eco-driving) in the energy management problem. The work focus on micro trip scenarios, such as signalized intersections. Hu et al. [22] propose a model predictive control concept to extend the lifetime of a fuel cell electric bus. The degradation of both fuel cell and battery systems is considered quantitatively. Wu et al. [23] show that when strategies are optimized for a given driving cycle, they have similar performances. However, for unknown cycles, the results differ in a significant way. Hu et al. [24] investigate the multi-objective optimization of the hydrogen economy and system lifetime by simultaneously optimizing the powertrain design and energy management. The durability of the fuel cell system is evaluated using the heuristic degradation model proposed in [9]. Similarly, Liu et al. [25] optimize the powertrain size using Pontryagin's minimum principle to minimize the hydrogen consumption. However, in this case, the fuel cell lifetime is neglected, and the multi-objective target focuses on the extension of the battery life.

The present work investigates the energy management of heavy-duty fuel cell vehicles for road freight transportation in real-world driving scenarios, filling the literature gaps mentioned earlier. Here, the vehicle operation is represented realistically through a total of 1750 h of real-world driving data, including speed and elevation. Moreover, the vehicle mass is variable between 14 and 40 tonnes depending on the cycles, which is typical of road freight transportation due to variable loading conditions. The vehicle performances are evaluated in terms of the hydrogen economy and system lifetime adopting six EMSs with different goals and motivations. Firstly, Pontryagin's minimum principle is used to find the hydrogen economy's theoretical limit, considering the complete knowledge of the driving cycles. However, this work's ultimate purpose is to investigate strategies that can be practically implemented in a real vehicle. Thus, an equivalent consumption minimization strategy is designed to evaluate the feasibility of the hydrogen economy optimization using only past driving information. The study then focuses on the investigation of the potential benefits and drawbacks of heuristic, optimal, and predictive energy management methods for the multi-objective optimization of the hydrogen economy and system lifetime. To this end, rule-based, nonlinear programming, and model predictive control strategies are designed. The first two are optimally tuned using an evolutionary algorithm to express their maximum potential. For the same reason, the predictive strategy uses exact knowledge of the future driving conditions rather than considering a system to predict them. Finally, Pontryagin's minimum principle is applied to investigate its use as a benchmark for the multi-objective optimization of the hydrogen economy and system lifetime, which was never studied before.

Eventually, the extensive and realistic representation of the vehicle operation determines a robust design of energy management strategies. The effectiveness and robustness of the results are evaluated globally to ensure a fair comparison of the strategies and statistically to highlight the importance of considering a large number of driving cycles. The comparison between the six strategies provides a good understanding of the potential benefits and drawbacks of the different energy management methods and targets.

The remainder of the paper is structured as follows. Section 2 outlines the vehicle model, which is essential for the formulation of the energy management problem. Section 3 provides information about the real-world driving cycles that determine the realistic representation of the vehicle operation. Section 4 defines a framework for the statistical evaluation of the results. Section 5 describes the six energy management strategies under investigation. Section 6 compares and analyzes the simulation results. Finally, Section 7 concludes this work.

2. Vehicle modeling

The vehicle modeling approach can be either forward or backward facing [26]. The latter assumes that the vehicle always meets its target performance to follow the speed profile strictly. Speed, acceleration, and road slope are used to calculate the power required to drive the vehicle without checking against the actual powertrain capabilities. On the other hand, the forward approach includes a driver model, which generates a power request by comparing actual and target speed. In this case, if the powertrain cannot provide the requested power, the vehicle slows down, deviating from the target speed.

This work considers the backward approach to ensure a fair comparison between the energy management strategies. Indeed, the forward approach determines different load profiles for the same cycle depending on the energy management, and, thus, it introduces a bias on the hydrogen consumption. For example, the consumption would be lower by avoiding power peaks, but the driving cycle longer (i.e., slower truck). In general, fuel cell and battery systems have complex dynamics and require detailed modeling. However, this work considers simplified models that neglect dynamic behaviors within the systems. This choice is in accord with using the backward modeling approach and provides adequate accuracy for a system-level analysis.

The heavy-duty vehicle considered in this work includes a fuel cell system with a nominal power of 300 kW and a battery system with an energy capacity of 76 kWh. Fig. 1 depicts the architecture of the electric powertrain under investigation. The electric motor and the fuel cell system are connected to a DC bus through power converters, whereas the battery system is directly linked to it. The parameters of the following vehicle model correspond to those adopted in [11], and they are all listed in Table 2.

2.1. Vehicle dynamics

Fig. 2 depicts the longitudinal dynamics of the vehicle. The resistant forces acting on the vehicle are associated with rolling friction (1a), road slope (1b), and aerodynamic drag (1c). Thus, the total resistant force (1d) changes during the driving cycle depending on speed v and road slope α. Because of the large mass m_v of road freight vehicles, the force F_{slope} significantly affects the load. Therefore, the road slope cannot be neglected as usually assumed for light-duty vehicles.

$$F_{roll} = m_v \; g \; c_r \; \cos\alpha \tag{1a}$$

$$F_{slope} = m_v \; g \; \sin\alpha \tag{1b}$$

$$F_{drag} = 1/2 \; A_v \; c_x \; \rho_{air} \; v^2 \tag{1c}$$

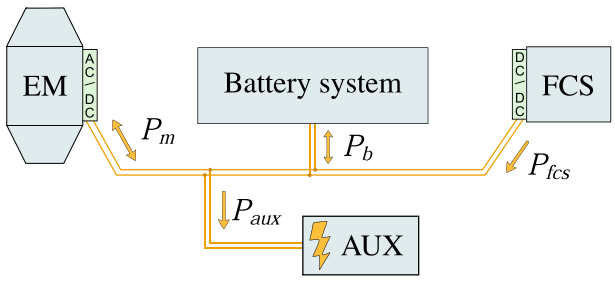

Fig. 1. Architecture of the electric powertrain of the vehicle. Legend: electric motor (EM), auxiliary systems (AUX), and fuel cell system (FCS).

$$F_{res} = F_{roll} + F_{slope} + F_{drag} \tag{1d}$$

The backward approach allows to calculate the power at wheels P_w that determines the acceleration $\dot{v}$ as follows.

$$P_w = (m_v\ \dot{v} + F_{res})\ v \tag{2}$$

The exact modeling of the power losses related to the electric motor, power converters, and drivetrain components is not relevant to this work's purposes. Here, an average total efficiency η_T is used to calculate the electric motor power P_m.

$$P_m = P_w\ \eta_T^{-\mathrm{sgn}(P_w)} \tag{3}$$

Finally, the total electric load P_{el} is calculated in (4) also considering the auxiliary loads P_{aux} (e.g., cooling trucks, air conditioning). For simplicity, these loads are assumed constant.

$$P_{el} = P_{aux} + P_m \tag{4}$$

2.2. Fuel cell system

A fuel cell system includes one or multiple stacks and auxiliary components, e.g., air compressor, humidifiers, recirculation, and cooling pumps [27]. Stacks are connections of individual fuel cells in series to achieve higher voltage and power.

The operation of a fuel cell depends on many variables. The most significant are current, temperature, relative humidity, and partial pressure of reactants. Detailed modeling of stacks and auxiliary components is required to capture the complex dynamics of fuel cell systems. Additionally, the operation highly depends on the low-level control logic, which is not considered in this work. References to dynamic models with different detail levels can be found in [27–31].

This work considers a simplified quasi-static model. Here, the fuel cell system power P_{fcs} is intended as the difference between stack power and auxiliaries losses.

$$P_{fcs} = P_{fcs,stack} - P_{fcs,aux} \tag{5}$$

The power converter linking the fuel cell system to the DC bus is assumed to be ideal and, thus, the corresponding losses are neglected. The specific hydrogen consumption, μ_{H_2}, is defined in (6) and the absolute one, $\dot{m}_{H_2}$, in (7). The hydrogen lower heating value is denoted with LHV_{H_2} and the system efficiency with η_{fcs}. Because of the simplified modeling approach considered in this work, the hydrogen consumption depends only on the power, as shown in Fig. 3. Further details about the efficiency characteristic cannot be provided because of a confidentiality agreement. However, the values shown in Fig. 3 are similar to the ones shown in [32], confirming that it is an authentic representation of a real fuel cell system.

$$\mu_{H_2} = \left(\eta_{fcs}\ LHV_{H_2}\right)^{-1} \tag{6}$$

$$\dot{m}_{H_2} = \mu_{H_2}\ P_{fcs} \tag{7}$$

2.3. Battery system

Fig. 4 depicts the equivalent circuit considered to model the battery system. The open-circuit voltage source V_{oc} is connected in series with the internal resistance R_{int}. The battery power P_b is expressed as in (8), where the terminal voltage V_b is calculated by applying Kirchhoff's law. In this work, the battery current I_b is assumed positive during discharge.

$$P_b = V_b\ I_b = (V_{oc} - R_{int}\ I_b)\ I_b \tag{8}$$

Inverting the formula above, the battery current can be expressed as a function of the power, as follows.

$$I_b = \frac{V_{oc} - \sqrt{V_{oc}^2 - 4\ P_b\ R_{int}}}{2\ R_{int}} \tag{9}$$

For simplicity, the open-circuit voltage and internal resistance of the battery are assumed constant. The ohmic losses P_Ω are calculated depending on the current.

$$P_\Omega = R_{int}\ I_b^2 \tag{10}$$

The battery state of charge SoC is defined as the ratio between actual and nominal charge, Q and Q_{nom}.

$$SoC = \frac{Q}{Q_{nom}} \tag{11}$$

The SoC rate of change is calculated as in (12), assuming the nominal charge constant, for simplicity. The charge derivative corresponds by definition to the electric current. Using (9), the state of charge dynamics can be expressed as a function of battery power.

$$\dot{SoC} = \frac{\dot{Q}}{Q_{nom}} = \frac{-I_b}{Q_{nom}} = -\frac{V_{oc} - \sqrt{V_{oc}^2 - 4\ P_b\ R_{int}}}{2\ R_{int}\ Q_{nom}} \tag{12}$$

2.4. Constraints

In this work, the fuel cell power has a lower bound, $P_{fcs,idle}$, to force idle operation. Thanks to this constraint, fuel cell shutdowns and low-power operations are prevented, limiting the degradation. The upper bound is the nominal power $P_{fcs,nom}$.

$$P_{fcs,idle} \leqslant P_{fcs} \leqslant P_{fcs,nom} \tag{13}$$

The battery power is constrained to the maximum charge and discharge values, $P_{b,ch}$ and $P_{b,dis}$. Note that because of the assumption on the battery current sign, the power is negative during charge.

$$P_{b,ch} \leqslant P_b \leqslant P_{b,dis} \tag{14}$$

The electric load is provided together by the fuel cell and battery systems, and it is calculated as follows.

$$P_{el} = P_{fcs} + P_b \tag{15}$$

Using (15), it is possible to modify the fuel cell power constraint as in (16) so that the battery constraints are automatically satisfied. In this case, the fuel cell minimum and maximum power, $P_{fcs,min}$and $P_{fcs,max}$, depend on the electric load. The function *bound* saturates the second argument between the first (lower bound) and the third (upper bound).

$$P_{fcs,min} = \mathrm{bound}\left[P_{fcs,idle},\ \left(P_{el} - P_{b,dis}\right),\ P_{fcs,nom}\right] \tag{16a}$$

$$P_{fcs,max} = \mathrm{bound}\left[P_{fcs,idle},\ \left(P_{el} - P_{b,ch}\right),\ P_{fcs,nom}\right] \tag{16b}$$

$$P_{fcs,min} \leqslant P_{fcs} \leqslant P_{fcs,max} \tag{16c}$$

Table 2
Parameters of vehicle model.

Parameter	Symbol	Value
Gravitational acceleration	g	9.81 m/s^2
Rolling friction coefficient	c_r	0.01
Vehicle frontal area	A_v	8 m^2
Drag coefficient	c_x	0.35
Air density	ρ_{air}	1.2 kg/m^3
Auxiliary loads	P_{aux}	10 kW
Total efficiency	η_T	0.80
Hydrogen lower heating value	LHV_{H_2}	120 MJ/kg
Open-circuit voltage	V_{oc}	380 V
Internal resistance	R_{int}	0.05 Ω
Nominal charge	Q_{nom}	200 Ah
Idle power	$P_{fcs,idle}$	30 kW
Nominal power	$P_{fcs,nom}$	300 kW
Max charging power	$P_{b,ch}$	−150 kW
Max discharging power	$P_{b,dis}$	300 kW

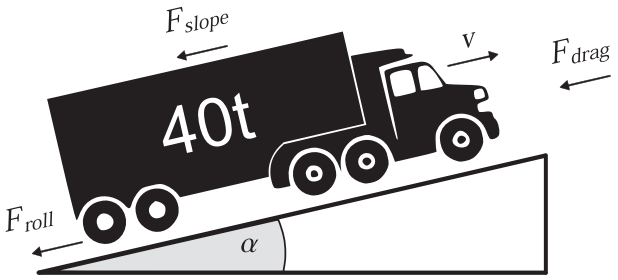

Fig. 2. Scheme of vehicle longitudinal dynamics.

The electric load is saturated between the powertrain capabilities through (17) to neglect the mechanical braking power and eventual load spikes deriving from real-world driving cycles.

$$P_{el} = \text{bound}\left[\left(P_{fcs,idle} + P_{b,ch}\right), P_{el}, \left(P_{fcs,nom} + P_{b,dis}\right)\right] \quad (17)$$

3. Real-world driving cycles

This work considers real-world driving data of heavy-duty vehicles for road freight transportation, recorded for two months in a fleet of fifteen conventional trucks operating in Central Europe. The data includes latitude, longitude, and elevation of the vehicle, with a sampling time of 1 s. Central Europe is particularly challenging for road freight vehicles because of many hills and mountains. Fig. 5 shows the geographic distribution of the recorded data on the region's elevation map.

A criterion was defined for the systematic identification of driving cycles: a cycle ends when the vehicle stops for more than 5 min. This procedure resulted in a set of cycles that was still too large to be considered entirely. Therefore, a subset was selected considering only the cycles at least two hours-long and with limited stopping time.

In the end, this work considers 544 cycles for the energy management investigation, amounting to a total of 1750 driving hours and 141,000 km. The top six tiles of Fig. 6 are boxplots of interesting driving features of these cycles. Duration, average speed, and traveled distance are straightforward. The relative positive acceleration (RPA), calculated as in (18), is a dynamic driving metric typically used to analyze real

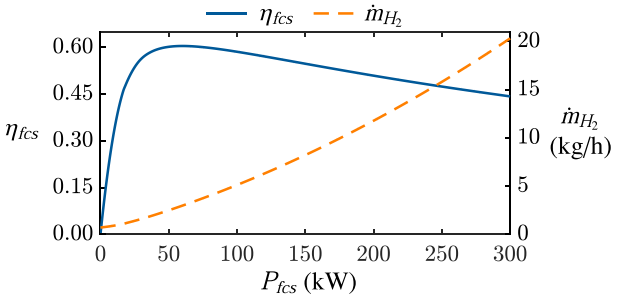

Fig. 3. Fuel cell system efficiency and hydrogen consumption.

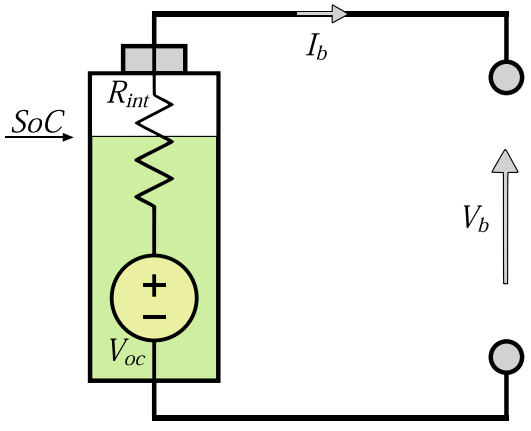

Fig. 4. Equivalent circuit of the battery system.

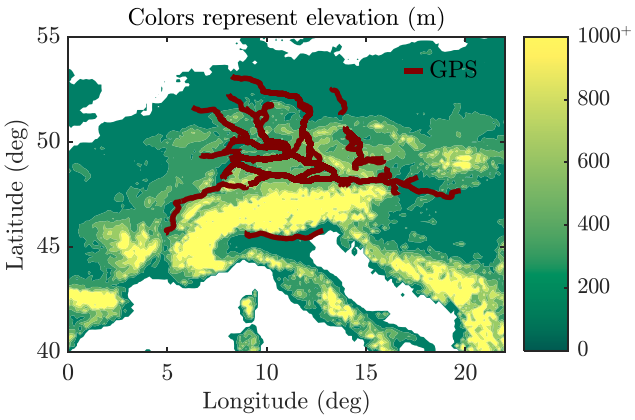

Fig. 5. Geographic distribution of recorded driving data.

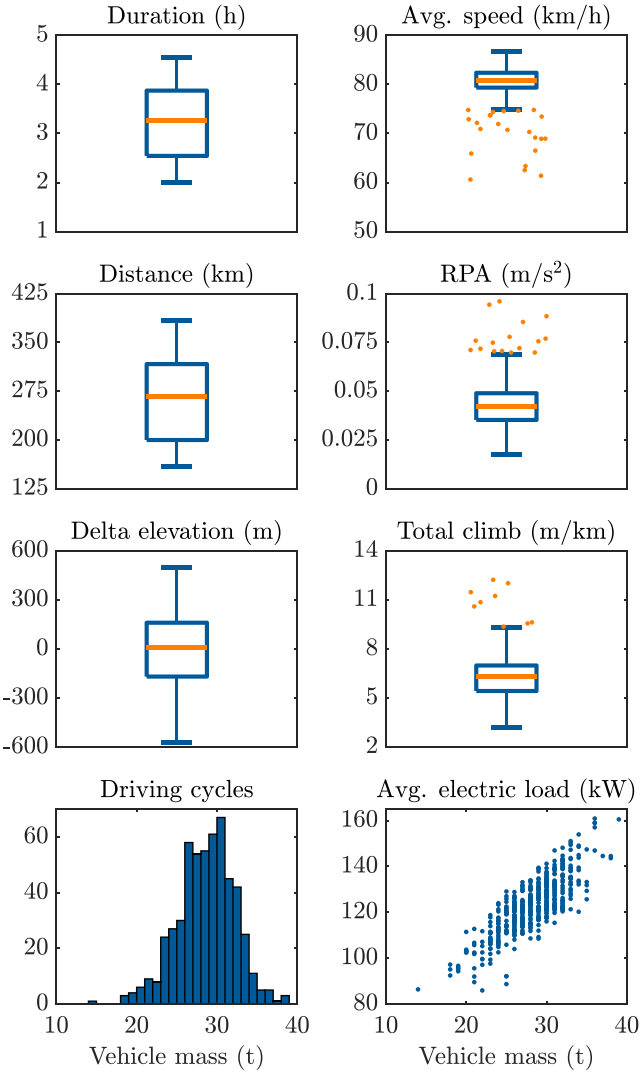

Fig. 6. Statistical representation of interesting driving features.

driving emissions cycles. Moreover, Braun et al. [33] find a high correlation between RPA and battery electric vehicles' energy consumption.

$$\mathrm{RPA} = \frac{\int v \cdot a^{+} dt}{\int v \; dt} \tag{18}$$

In Fig. 5, delta elevation refers to the difference between ending and starting values, whereas the total climb is calculated summing only positive elevation increments.

A key parameter in the vehicle dynamics is the vehicle's mass, m_v, which changes according to the truck loading conditions. In this work, it is known that all trucks in the fleet have a maximum weight capacity of 40 tonnes, but no information about the actual loading was recorded. A method is adopted to estimate the vehicle's mass to overcome this limitation, assuming that the vehicle is accelerated using the maximum power for a specific time in each cycle. In particular, the mass is estimated such that P_w exceeds 400 kW for 0.5% of the cycle's duration, rounding to the closest tonne. The bottom tiles of Fig. 6 show the estimated vehicle mass and its impact on the average electric load. Overall, the massive amount of driving cycles and the variable loading create a realistic representation of road freight vehicles' annual operation, enabling the robust design of EMSs and a statistical evaluation of the results.

Fig. 7 shows the speed and elevation profiles of some representative driving cycles. The first one has the minimum RPA among all cycles and represents an extended and stable cruising at 90 km/h. On the contrary, the second cycle has the maximum RPA, and it represents a sub-urban driving with heavy traffic and frequent turns. The other cycles have the minimum and maximum climb and the minimum and maximum vehicle mass.

4. Performance indexes

In fuel cell electric vehicles, energy management strategies have multiple goals: maximize the hydrogen economy and fuel cell lifetime, and sustain the battery charge. In this section, several indexes are defined to evaluate the effectiveness of EMS. The calculation of the total hydrogen consumption m_{H_2} is straightforward.

$$m_{H_2} = \int \dot{m}_{H_2} \; dt \tag{19}$$

As detailed in Section 1, reducing fuel cell transients is the main target to extend lifetime: rapid fuel cell power changes result in high lifetime consumption. Therefore, a first degradation meaningful index is the standard deviation of the fuel cell power rate of change $\sigma(\dot{P}_{fcs})$. A second index is defined in this work as an equivalent lifetime consumption, m_L, as follows.

$$m_L = \int w_L \; \dot{P}_{fcs}^{2} \; dt \tag{20}$$

The conversion factor w_L is the weight of system lifetime relative to the hydrogen economy. The larger this factor is, the more dominant the lifetime target becomes. In this work, a good trade-off between the goals is found choosing the conversion factor as: $w_L = 5.56 \times 10^{-12}$ kg·s·W^{-2}. Section 6 shows that this value is sufficiently high to determine a significant change in fuel cell transients without affecting the hydrogen economy. It must be noted that m_L is proportional to the square of $\sigma(\dot{P}_{fcs})$ because the average of $\dot{P}_{fcs}$ is zero. However, introducing m_L allows defining a multi-objective total cost J in (21), as the sum of hydrogen and lifetime consumptions. This index can be conveniently used as the target of the optimal strategies.

$$J = m_{H_2} + m_L \tag{21}$$

The voltage loss due to potential cycling defined in [9] is used in the present work as an additional degradation index. The voltage loss, denoted with ΔV_{fcs}, is proportional to the number of equivalent load cycles, and it is calculated as follows.

$$\Delta V_{fcs} = 1.72{\cdot}0.0000593\%{\cdot}\frac{\int \left|\dot{P}_{fcs}\right| \; dt}{P_{fcs,\,nom}} \tag{22}$$

The battery operation is analyzed through the average state of charge, $\overline{SoC}$, and its standard deviation $\sigma(SoC)$. The equivalent number of charge–discharge cycles, N_b, holds important information related to battery aging [22]. This value is calculated considering the total charge variation as follows.

$$N_b = \frac{\int \left|\dot{Q}\right| \; dt}{2 \; Q_{nom}} \tag{23}$$

The indexes defined in this section are used to analyze the effectiveness of the energy management strategies under investigation. The results are evaluated considering the driving cycles in two ways: as a sequence and individually. The first approach yields a global evaluation, whereas the second a statistical one.

4.1. Analysis on sequence of cycles

All driving cycles are considered in a random but fixed sequence. At the end of a cycle, the battery state of charge is the initial one for the next cycle. The fuel cell system is shut down at the end of each cycle to simulate a real-world scenario where the vehicle is stopped for a considerable time. Depending on the random sequence, the vehicle mass can either change or stay constant between cycles. In the first case, the stop corresponds to loading/unloading operations. Otherwise, the stop is for refueling or mandatory resting for the driver. This representation of the truck operation yields a realistic global evaluation of the results.

4.2. Analysis on individual cycles

The EMS performance is also analyzed considering each cycle individually. In this case, the variation between the initial state of charge, SoC_I, and the final one, SoC_F, affects the hydrogen consumption. For example, if the battery is charged during the cycle, higher consumption is expected. Thus, to compare the results of different energy management strategies fairly, the hydrogen consumption must be corrected depending on the battery charge change.

The underlying idea behind the correction terms defined in this work is that the fuel cell roughly has to cover for the average electric load and ohmic losses to sustain the battery's charge. First, the energy associated to the SoC variation is converted in equivalent hydrogen mass, $m_{H_2,\,b}$, as in (24). Here, the sum of the average load $\overline{P}_{el}$ and ohmic losses $\overline{P}_{\Omega}$ is used to calculate the specific consumption $\overline{\mu}_{H_2}$ for the conversion.

$$\overline{\mu}_{H_2} = \mu_{H_2}\left(\overline{P}_{el} + \overline{P}_{\Omega}\right) \tag{24a}$$

$$m_{H_2,\,b} = \overline{\mu}_{H_2}\left(SoC_I - SoC_F\right) \; V_{oc} \; Q_{nom} \tag{24b}$$

A second correction term, $m^{*}_{H_2}$, is calculated as in (25). This term considers that the fuel cell operation changes depending on the SoC variation. For example, to charge the battery the fuel cell operates at higher average power $\overline{P}_{fcs}$ and specific consumption $\widetilde{\mu}_{H_2}$.

$$\widetilde{\mu}_{H_2} = \mu_{H_2}\left(\overline{P}_{fcs}\right) \tag{25a}$$

$$m^{*}_{H_2} = \left(\overline{\mu}_{H_2} - \widetilde{\mu}_{H_2}\right) \int P_{fcs} \; dt \tag{25b}$$

Using the correction terms $m_{H_2,\,b}$ and $m^{*}_{H_2}$, the hydrogen consumption becomes almost independent from the SoC change during the cycle. Note that when $SoC_F = SoC_I$, the first correction term is zero by definition,

whereas the second is negligible because $\overline{\mu}_{H_2}$ becomes approximately equal to $\widetilde{\mu}_{H_2}$. Finally, the corrected hydrogen cost is denoted with J_H and calculated as follows.

$$J_H = m_{H_2} + m_{H_2,b} + m^*_{H_2} \tag{26}$$

The total multi-objective cost for individual cycles is denoted with $J_{H\&L}$ and defined as follows, similarly to (21).

$$J_{H\&L} = J_H + m_L \tag{27}$$

Here, the subscript $H\&L$ denotes the multi-objective target of hydrogen economy and system lifetime, whereas H the hydrogen economy as an individual target.

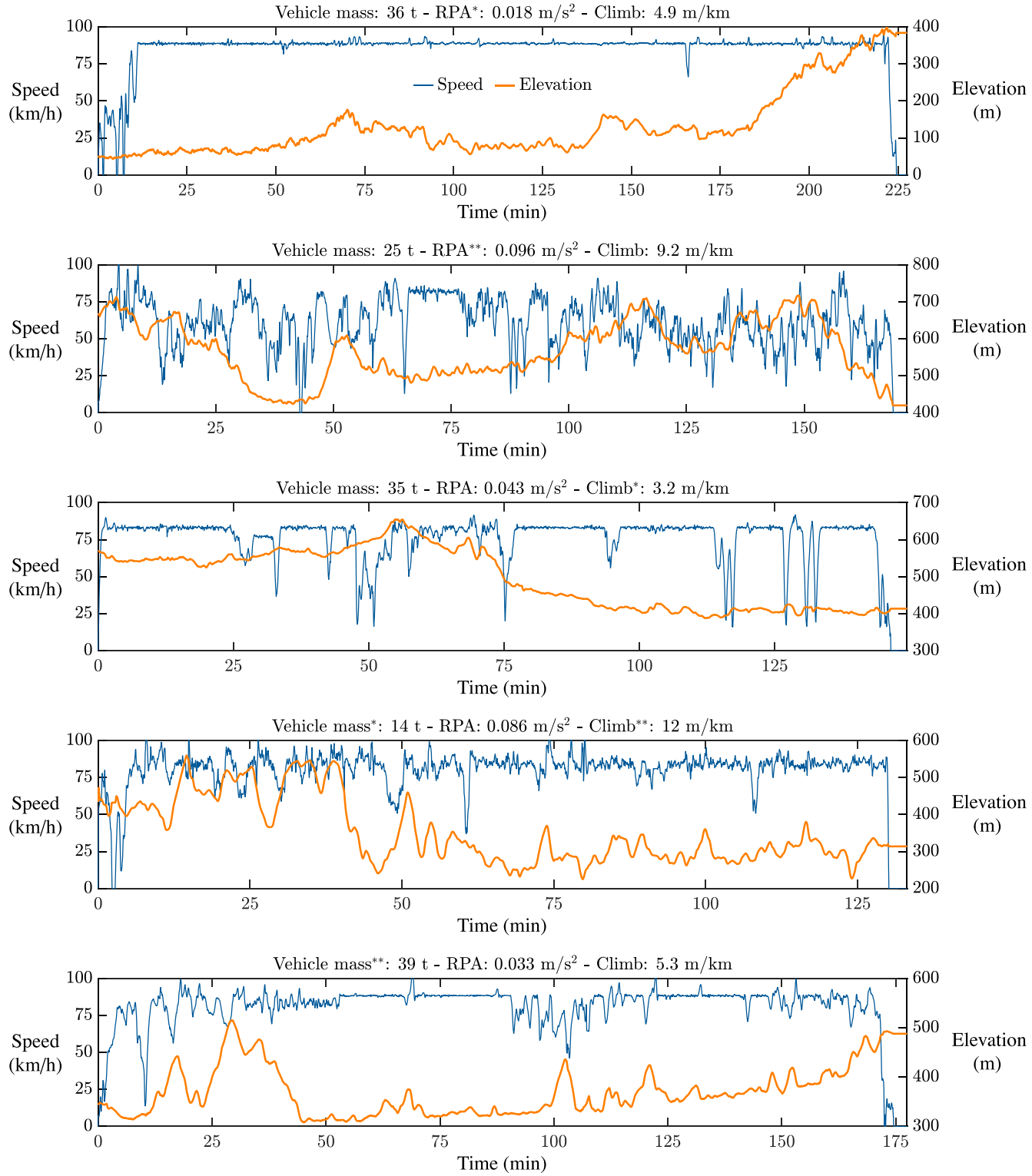

Fig. 7. Speed and elevation profiles of five driving cycles. * indicates the minimum value and ** the maximum.

5. Energy management strategies

This work aims to design strategies that can be practically implemented in a real vehicle, evaluating the results in terms of the hydrogen economy and system lifetime. In total, six energy management strategies are investigated with different goals and motivations. Pontryagin's minimum principle finds the hydrogen economy's theoretical limit, considering the complete knowledge of the driving cycles. However, an equivalent consumption minimization strategy is designed to evaluate hydrogen economy optimization's feasibility using only past driving information. The remaining strategies investigate the potential benefits and drawbacks of heuristic, optimal, and predictive energy management methods for the multi-objective optimization of the hydrogen economy and system lifetime. Finally, Pontryagin's minimum principle is applied to study its use as a benchmark for the multi-objective optimization problem.

In the vehicle under investigation, the fuel cell and battery systems provide the electric load together as expressed by (15). Therefore, choosing the fuel cell power as the control variable, the battery power is determined depending on the electric load as in (28). For all the strategies, to ensure that the constraints are met accordingly to (16), the fuel cell power is always bounded using (29) in the final step of the energy management strategies.

$$P_b = P_{el} - P_{fcs} \tag{28}$$

$$P_{fcs} = \text{bound}\left[P_{fcs,min},\, P_{fcs},\, P_{fcs,max}\right] \tag{29}$$

The following of this section details the formulation of the six energy management strategies.

5.1. Pontryagin's minimum principle

The optimal control theory aims to minimize a performance index defined as in (30). The instantaneous cost function L generally depends on system states x and controls u.

$$C = \int L\left(x, u, t\right)\, dt \tag{30}$$

Pontryagin's minimum principle (PMP) is defined as a set of necessary but not sufficient conditions for optimality [34]. The principle is based on the ancillary function H, known as Hamiltonian, defined as follows.

$$H(x, u, t, \lambda) = L(x, u, t) + \lambda \cdot \dot{x}(x, u) \tag{31}$$

This function combines state dynamics and cost function through the *co-state* λ. From a physical standpoint, the Hamiltonian can be interpreted as an augmented cost that considers positive or negative state changes. According to Pontryagin's minimum principle, optimal controls always minimize the Hamiltonian. Generally, the principle is not sufficient for optimality, and it cannot be used directly to find optimal control laws. However, in some problems, the principle can be sufficient for optimality. The controls u^* that minimize the Hamiltonian are called extremal. Using the PMP formulation defined in (32) in each time instant, the extremal control law can be found.

$$u^* = \underset{u}{\text{argmin}}\;\; H\left(x, u, t, \lambda\right) \tag{32a}$$

$$\dot{x} = \left.\frac{\partial H}{\partial \lambda}\right|_{u^*} \tag{32b}$$

$$\dot{\lambda} = -\left.\frac{\partial H}{\partial x}\right|_{u^*} \tag{32c}$$

Serrao et al. [35] compare PMP and dynamic programming to minimize the fuel consumption of hybrid electric vehicles, proving that PMP is sufficient for the global optimality of the solution. On the other hand, the computational complexity of dynamic programming is significantly higher compared to PMP. For this reason, Pontryagin's minimum principle is usually preferred in comparison to dynamic programming as a benchmark strategy for energy management problems.

In the present work, PMP considers two different formulations of the cost function. Firstly, to minimize the hydrogen consumption (19). And secondly, for the minimization of the hydrogen and lifetime consumptions (21). While the first formulation was already investigated in the literature, the second one is studied for the first time.

5.1.1. PMP for hydrogen economy

This energy management strategy uses Pontryagin's minimum principle to calculate the minimum hydrogen consumption of the vehicle (19). The strategy is referred to as PMP_H in the remainder of the paper. In this formulation of the principle, the control variable is P_{fcs}, the state is *SoC*, and the cost function is the hydrogen consumption. Therefore, the Hamiltonian is defined as follows.

$$H = \dot{m}_{H_2}\left(P_{fcs}\right) + \lambda_0\;\; \dot{SoC}\left(P_{el}, P_{fcs}\right) \tag{32d}$$

The optimal fuel cell power P^*_{fcs} is found among the set U of controls that meet the constraints (16), by applying PMP as formulated in (34). Considering that the Hamiltonian defined in (32d) does not depend on the *SoC*, it follows from (32c) that the co-state is constant. As such, it is denoted with λ_0 in (34c).

$$P^*_{fcs}(P_{el}, \lambda_0) = \underset{P_{fcs} \in U}{\text{argmin}}\;\; H\left(P_{el}, P_{fcs}, \lambda_0\right) \tag{34a}$$

$$\dot{SoC} = -\frac{V_{oc} - \sqrt{V_{oc}^2 - 4\,\left(P_{el} - P^*_{fcs}\right)\,R_{int}}}{2\,R_{int}\,Q_{nom}} \tag{34b}$$

$$\dot{\lambda} = 0 \longrightarrow \lambda = \lambda_0 \tag{34c}$$

In this work, the Hamiltonian is minimized numerically by discretizing the control set U, using 200 W as grid-spacing. The minimum of the Hamiltonian is always unique and, thus, the optimal control value P^*_{fcs} only depends on the electric load and the co-state, as shown in Fig. 8. Here, two extreme cases can be noted: the orange line corresponding to $\lambda_0 = -8$ and the blue line to $\lambda_0 = -2$. In the first case, the fuel cell always operates at the maximum power allowed (not to cause violation of the battery constraints). In the second, always at the minimum. Fig. 8 helps to understand how the co-state value affects the fuel cell operation and, therefore, the battery charge at the end of the driving cycle: the lower λ_0, the higher charge. PMP is an offline strategy because the co-state value must be found iteratively until the final battery charge reaches its assigned target within a certain tolerance. In this work, the final target is always fixed as $SoC_F = 0.50$ and the tolerance to 0.005. It must be noted that to avoid complete charge or discharge of the battery, it is

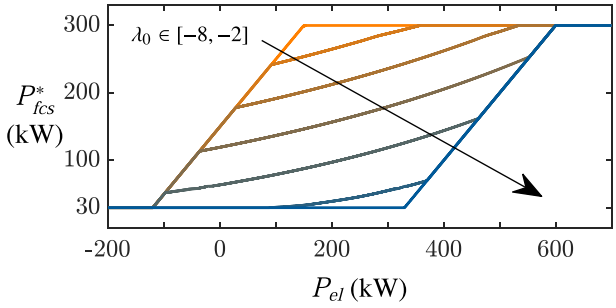

Fig. 8. Optimal fuel cell power dependency on electric load and co-state according to (34a). The orange line corresponding to $\lambda_0 = -8$ and the blue line to $\lambda_0 = -2$. (For interpretation of the references to colour in this figure legend, the reader is referred to the web version of this article.)

possible to add penalty functions in the formulation of the Hamiltonian (e.g., as in [14]). However, penalty functions might affect the optimality of the solution. In the present work, no additional term was considered in the formulation of the Hamiltonian because in no case the battery was ever fully charged or discharged during the simulations.

5.1.2. PMP for hydrogen economy and system lifetime

This energy management strategy uses Pontryagin's minimum principle to minimize the multi-objective performance index (21). The strategy is referred to as $PMP_{H\&L}$ in the remainder of the paper. The optimal fuel cell power is still calculated using in (34), but considering the Hamiltonian defined in (35). Here, the first two terms on the right-hand side correspond to the instantaneous cost of (21).

$$H = \dot{m}_{H_2} + w_L \ \dot{P}_{fcs}^2 + \lambda_0 \ \dot{SoC} \tag{35}$$

This work wants to prove that the application of Pontryagin's minimum principle is not sufficient for the multi-objective optimization of hydrogen and lifetime consumption. If the comparison with other strategies shows that better results can be achieved, it will be evident that the principle is not sufficient for global optimality.

5.2. Model predictive control

Model predictive control (MPC) refers to a broad framework of control strategies that use a system model to predict its future outputs and find optimal controls. Ferrara et al. propose a predictive energy management concept in [11], using instantaneous and successive linearizations of the vehicle model to formulate an optimization problem that can be solved with quadratic programming. The optimal controls are found to minimize a quadratic cost function over a finite time horizon, which includes terms related to future inputs and outputs.

This work considers and adapts the strategy proposed in [11] by using a new formulation of the cost function and changing the system's outputs accordingly. The reader is addressed to the reference for further details on the predictive management concept. The new cost function, J_{MPC}, is defined in (36) considering a predictive time horizon of 10 s and a sample time of 1 s. It is important to note that the cost function defined in (36) differs from the one in (21), but the underlying goals are the same. In particular, the first term on the right-hand side aims to maximize the hydrogen economy operating the fuel cell system at its maximum efficiency (i.e., $\eta_{fcs} = 0.61$), the second to reduce fuel cell transients, and the third to guarantee the battery charge sustaining. The MPC considers a regression model of the efficiency shown in Fig. 3 as the ratio of a sixth-order polynomial and a first-order one. The parameters of the cost function are heuristically tuned as: $m_1 = 2 \times 10^{-11}$, $m_2 = 12$, and $m_3 = 0.65$. The predictive horizon and the tuning were fixed once a satisfying trade-off between accuracy and simulation time was reached.

$$J_{MPC} = \sum_{k=1}^{10} \left(\eta_{fcs,k} - 0.61\right)^2 + m_1 \cdot \dot{P}_{fcs,k}^2 + m_2 \cdot \left(m_3 - SoC_k\right)^2 \tag{36}$$

This strategy requires predictive driving information to calculate the electric load in the next 10 s. However, this work assumes that the load is precisely known over the predictive horizon to investigate MPC's maximum potential for the multi-objective optimization of the hydrogen and lifetime consumption. Nevertheless, after establishing the potential benefits, further investigations will be required to confirm the strategy's effectiveness when considering uncertain driving information to predict the future load. For example, a speed forecasting method based on Markov chain could be used as in [36].

5.3. Equivalent consumption minimization strategy

An equivalent consumption minimization strategy (ECMS) is designed as an online implementation of PMP_H. Indeed, in (32d), the Hamiltonian can be interpreted as the sum of two fuel consumptions. From this perspective, the co-state acts as an equivalence factor, λ_{ECMS}, transforming the battery current in equivalent hydrogen consumption.

$$H = \dot{m}_{H_2} + \lambda_{ECMS} \ \dot{SoC} \tag{37}$$

The strategy differs from PMP_H only because of the equivalence factor. Whereas, the optimal fuel cell power is calculated minimizing the Hamiltonian in the same way as in (34).

The equivalence factor must be calculated online using the available information. In this work, a simple but effective method for the calculation of λ_{ECMS} is proposed to achieve high hydrogen economy. In PMP_H, the co-state value depends mostly on the average electric load and *SoC* target as it can be seen from Fig. 9, which shows the co-states λ_0^* such that: $SoC_F = SoC_I = 0.50$. A simple linear regression can model the relation between λ_0^* and the average load $\overline{P}_{el}$ with high accuracy.

$$\lambda_0^*\left(\overline{P}_{el}\right) = -2.93 - 1.49 \times 10^{-5} \ \overline{P}_{el} \tag{38}$$

Ideally, knowing the average electric load of the driving cycle beforehand, the equivalence factor could be calculated using (38). The *SoC* deviation from the initial value would be negligible, and the hydrogen economy would be maximum. However, this is not possible in reality because online EMSs cannot know the average load beforehand. In alternative, the initial equivalence factor is set to default as: $\lambda_{ECMS} = -5$. This value is reasonably chosen by analyzing the results reported in Fig. 9. Then, the equivalence factor is updated evaery e_1 seconds using (38), (39), and (40). In particular, the first term on the right-hand side of (40) is the average electric load. Whereas, the second one adds or subtracts power to recharge or discharge the battery, using e_2 as a weighting term and e_3 as a *SoC* reference. The values of the parameters e_i are listed in Table 3.

$$\lambda_{ECMS} = \lambda_0^*\left(P_{ECMS}\right) \tag{39}$$

$$P_{ECMS} = \frac{1}{t}\int_0^t P_{el} \ dt + e_2 \ \left(e_3 - SoC\right) V_{oc} \ Q_{nom} \tag{40}$$

5.4. Nonlinear programming

This strategy is designed as a simplified implementation of MPC. In this case, an optimization problem is formulated based on the instantaneous minimization of the nonlinear cost function defined in (41). The formulation of the cost derives from the one proposed for MPC in Section 5.2, with the same goals of the hydrogen economy, system lifetime, and battery charge sustaining. Here, the fuel cell power is calculated by minimizing the cost function J_{NLP} as in (42), using nonlinear programming. Thus, the strategy is referred to as NLP in this work. The values of the parameters n_i are listed in Table 3.

$$J_{NLP} = \left(\eta_{fcs} - 0.61\right)^2 + n_1 \ \dot{P}_{fcs}^2 + n_2 \ \left(n_3 - SoC\right)^2 \tag{41}$$

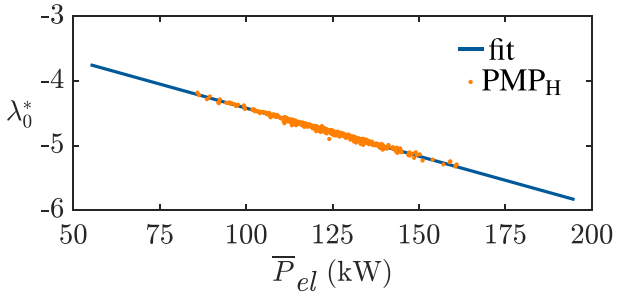

Fig. 9. Co-state values depending on the average electric load of driving cycles. The results refer to PMP_H, considering $SoC_F = SoC_I = 0.50$. The goodness of the fit is proved by the high coefficient of determination: $R^2 = 0.99$.

Table 3
Parameters of energy management strategies tuned using PSO.

	$i=1$	$i=2$	$i=3$	$i=4$
e_i	60	6.63×10^{-4}	0.502	
n_i	1.14×10^{-11}	72.8	0.670	
r_i	0.380	1.06×10^{-3}	0.685	3540

$$P_{fcs} = \underset{P_{fcs}\in U}{\operatorname{argmin}} \; J_{NLP}\left(P_{el}, P_{fcs}, SoC\right) \tag{42}$$

Contrary to MPC, this strategy does not require predictive driving information because the cost function is minimized instantaneously rather than over a future time horizon. Therefore, the comparison between MPC and NLP offers a direct evaluation of the benefits (i.e., effectiveness) and drawbacks (i.e., computational complexity) of predictive energy management. Nevertheless, in general, NLP is a compelling concept for energy management because it is also highly flexible, and it can be adapted to take into account additional objectives by suitably defining the cost function in (41).

5.5. Rule-based

This heuristic strategy is designed to have the lowest possible complexity. The rules defined in (43) calculate the fuel cell power. Thus, the strategy is referred to in this work as RB. The underlying idea is to operate the fuel cell system close to the maximum efficiency power: $P_{fcs,\eta_{max}} = 60$ kW.

$$P_{fcs} = P_{fcs,\eta_{max}} + r_1 \left(P_{el} - P_{fcs,\eta_{max}}\right) + r_2 \left(r_3 - SoC\right) V_{oc} \, Q_{nom} \tag{43a}$$

$$\text{subject to :} \quad |\dot{P}_{fcs}| \leqslant r_4 \tag{43b}$$

The second term on the right hand side of (43a) considers the load deviation from $P_{fcs,\eta_{max}}$. The third term considers the SoCdeviation from the reference r_3. The rate of change of the fuel cell power is limited to r_4 in (43b), to mitigate degradation phenomena. The values of the parameters r_i are listed in Table 3.

5.6. Optimization of EMS parameters

The EMS parameters of the online strategies are optimized using the particle swarm optimization (PSO) algorithm available in MATLAB's Optimization Toolbox [37]. This method ensures a fair comparison of the strategies eliminating any bias due to heuristic tunings. In particular, PSO is an evolutionary algorithm capable of finding optimal parameters by minimizing a suitably defined fitness function through a stochastic search [38].

In this work, the PSO's settings are left to the default values as in [37], but the swarm size is set to 25 elements. The strategies are tuned using the following procedure: first, two optimizations consider a random initialization of the swarm, then a third optimization includes the two sets of optimal parameters found previously.

All the optimizations consider a subset of 50 driving cycles out of the total 544 to analyze the strategies' effectiveness and robustness in unknown driving conditions. A penalty cost p is defined in (44) to ensure the battery's charge sustaining, using the average state of charge and its standard deviation. The coefficients are arbitrarily chosen, and the average SoC reference is set to 0.50. Moreover, if the battery is ever fully discharged, the penalty cost is set to infinite.

$$p = 100 \cdot \left| \overline{SoC} - 0.50 \right| + 400 \cdot \sigma\left(SoC\right) \tag{44}$$

The fitness function to be minimized, denoted with J_{PSO}, is defined below depending on the different objectives of the strategies. The performance indexes in (45) and (46) are calculated considering the 50 selected cycles in sequence. The results of the optimization are collected in Table 3.

$$\text{RB, NLP :} \quad J_{PSO} = p + J \tag{45}$$

$$\text{ECMS :} \quad J_{PSO} = p \cdot 0.50 + m_{H_2} \tag{46}$$

6. Simulation results

This section compares the energy management strategies under investigation considering the performance indexes defined in Section 4 for the analysis of the results. All the simulations are performed using MATLAB R2020a.

Using (29) in the final step of all strategies, the fuel cell power is such to always meet the battery power constraints and provide/regenerate the electric load entirely. Therefore, no further details about the compliance with the constraints are provided.

6.1. Analysis on the sequence of cycles

The global evaluation considers all driving cycles in sequence, as described in Section 4.1. In total, the truck drives 141,000 km in 1750 h, with variable loading conditions. The top half of Table 4 shows the overall results of the energy management strategies in absolute values. Whereas in the bottom half, each index is divided by its minimum value.

The strategies are sorted in ascending order considering the multi-objective cost J. MPC yields the best result and, in comparison, the value obtained with $\text{PMP}_{\text{H\&L}}$ is 17% higher. The application of Pontryagin's minimum principle is not sufficient to find global optimality for the multi-objective problem because there are strategies that yield better results. This outcome is motivated by the fact that the instantaneous minimization of the Hamiltonian cannot anticipate sharp load changes in any way, thus determining rapid fuel cell transients to deliver the electric load and meet the prescribed constraints. On the contrary, MPC involves the minimization of a cost function over a predictive horizon, which allows to consider and anticipate the load changes effectively, achieving a steadier operation of the fuel cell system. In particular, MPC yields a significantly lower lifetime consumption compared to the other strategies. Indeed, the multi-objective cost is 13% higher for RB and 14% for NLP, highlighting the potential of predictive energy management.

As expected, PMP_{H} yields the best result in terms of the hydrogen economy, confirming that this strategy can be effectively used to minimize fuel consumption. Notably, ECMS is exceptionally effective in minimizing the consumption using only past driving information and achieving a lower $\sigma(SoC)$. Indeed, the difference compared to PMP_{H} is smaller than the rounding error. RB and NLP use 2% more hydrogen than the theoretical minimum but have a significantly lower lifetime

Table 4
Global evaluation of energy management strategies. Top table: absolute values. Bottom table: each index is divided by its minimum value.

	J (t)	m_{H_2} (t)	m_L (t)	$\sigma(\dot{P}_{fcs})$ (kW/s)	ΔV_{fcs} (%)	$\sigma(SoC)$	N_b
MPC	13.3	12.1	1.2	5.8	7.2	0.06	920
RB	15.0	12.2	2.8	8.9	9.1	0.06	930
NLP	15.2	12.2	3.0	9.3	5.9	0.06	1040
$\text{PMP}_{\text{H\&L}}$	15.6	12.5	3.1	9.4	5.2	0.12	1040
PMP_{H}	18.7	12.0	6.7	13.9	19.1	0.10	970
ECMS	19.3	12.0	7.3	14.4	19.5	0.07	980
	J	m_{H_2}	m_L	$\sigma(\dot{P}_{fcs})$	ΔV_{fcs}	$\sigma(SoC)$	N_b
MPC	1	1.01	1	1	1.38	1	1
RB	1.13	1.02	2.33	1.53	1.75	1	1.01
NLP	1.14	1.02	2.50	1.60	1.13	1	1.13
$\text{PMP}_{\text{H\&L}}$	1.17	1.04	2.58	1.62	1	2.00	1.13
PMP_{H}	1.41	1	5.58	2.40	3.67	1.67	1.05
ECMS	1.45	1	6.08	2.48	3.75	1.17	1.07

consumption. MPC is also effective in terms of the hydrogen economy, with only a 1% deviation from the global optimum found by PMP_H.

Surprisingly, the fuel cell degradation indexes defined in this work are contrasting with each other: MPC has the minimum m_L and $\sigma(\dot{P}_{fcs})$, but not minimum ΔV_{fcs}. In general, RB and NLP show similar results between each other: the former has a slightly lower J, but the fuel cell degradation indexes are more balanced for the latter.

The comparison is fair due to the evaluation framework created in the previous sections. All the strategies determine an average battery state of charge equal to 50%. The standard deviation $\sigma(SoC)$ is similar for the optimally tuned strategies, thanks to the penalty term in the fitness function (44). Overall, the optimization of the EMS parameters using PSO is effective and a compelling feature to consider for future works on fuel cell vehicles' energy management. Remarkably, an optimally tuned heuristic strategy achieves better results than those of an optimal one.

In Section 1, the fuel cell operation in high-power conditions was not considered an active mitigation target because energy management strategies inherently avoid it to increase the system efficiency. For the sake of completeness, the simulation results show that the fuel cell operates above 90% of the nominal power for 0.2% of the total time using ECMS and PMP_H, 0.6% using MPC, 0.8% using NLP, 1.2% using RB, and 2.4% using $PMP_{H\&L}$.

6.2. Analysis on individual cycles

The evaluation of the results on individual cycles considers the performance indexes defined in Section 4.2. Additionally, the results of PMP_H and MPC are used to define two relative performance indexes, PI_H and $PI_{H\&L}$.

$$PI_H = J_{H,PMP_H} \,/\, J_H \tag{47}$$

$$PI_{H\&L} = J_{H\&L,MPC} \,/\, J_{H\&L} \tag{48}$$

Fig. 10 shows boxplots of the results for all cycles, providing valuable information about their variation range. Since PMP_H yields the theoretical minimum consumption, PI_H can be considered as an index of optimality in terms of the hydrogen economy. Similarly, $PI_{H\&L}$ cab be considered an index of effectiveness in terms of hydrogen economy and lifetime, even though MPC does not yield the theoretical minimum cost. The figure shows that the indexes vary largely depending on the cycles and, thus, it highlights the importance of considering the robust design framework presented in this work. Assuming for example that, rather than 544 driving cycles, it is only considered the one corresponding to the minimum $PI_{H\&L}$ of RB, that is 73%. This case would lead to a significant misjudgment of the strategy's effectiveness, as the median value is 88%. Fig. 10 also shows the contrasting behavior of the degradation indexes, ΔV_{fcs} and $\sigma(\dot{P}_{fcs})$.

To complete the analysis of individual cycles, Fig. 11 shows an example of the power-split obtained using NLP and the resulting SoCvariation. It can be noted that the fuel cell transients are limited, except during particular events. For example, at minute 6, the fuel cell power decreases rapidly to avoid violating the maximum battery charging power. Similarly, at minute 12.5, there is a rapid increase in the fuel cell power to meet the battery discharging constraint. It can also be noted that, around minute 9, a one-minute long uphill section determines a 5% discharge in the battery. This finding highlights how important and critical it is to consider the road elevation in heavy-duty vehicles. Indeed, long uphill sections can cause the battery's complete discharge and eventually force the vehicle to stop if the energy management strategy is not properly designed.

6.3. Analysis of minimum hydrogen consumption

In this section, the minimum hydrogen consumption is analyzed to provide interesting information on its dependency on the driving cycles' main features. The minimum consumption is found using PMP_H for each cycle ensuring that the battery charge is unchanged at the end ($SoC_F = SoC_I$). Fig. 12 shows the correlation between minimum consumption and the driving features described in Section 3. This analysis can be useful for future works on life cycle assessments of fuel cell trucks. As expected, the hydrogen consumption is highly correlated to the vehicle mass. However, the results are biased depending on whether the truck gains or loses elevation during the driving cycle. To eliminate this bias, the consumption is corrected in (49) considering the potential energy variation going from the elevation $z_I$to z_F. The equivalent consumption $\widetilde{m}_{H_2}$ shows an even higher correlation with the vehicle mass.

$$\widetilde{m}_{H_2} = m_{H_2} - \overline{\mu}_{H_2}\,(z_F - z_I)\; g\; m_v \tag{49}$$

The hydrogen consumption also depends on other driving features (e.g., road elevation, traffic, and driver). The bottom tiles show the consumption correlation with total climb and RPA. The consumption is expressed in tonne-kilometer (tkm), a standard measure of freight activity [2]. The results are natural: higher climb or traffic intensity (i.e.,

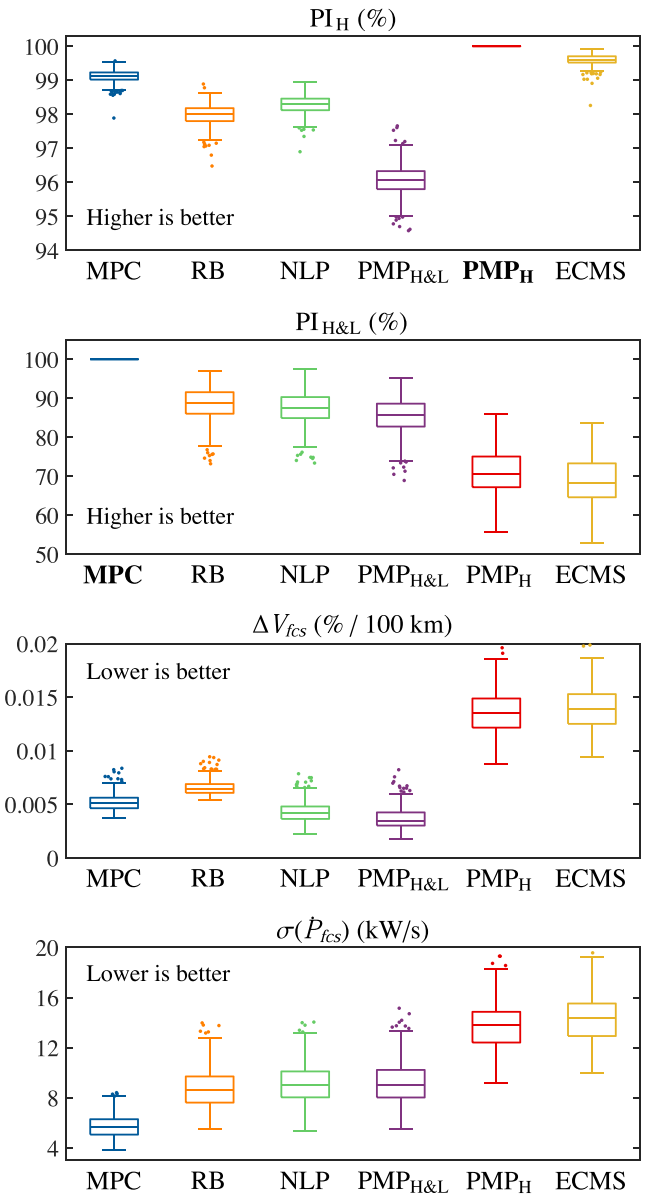

Fig. 10. Statistical evaluation and comparison of energy management strategies on individual cycles. The reference strategy for the relative performance index in the first tile is PMP_H, whereas in the second is MPC.

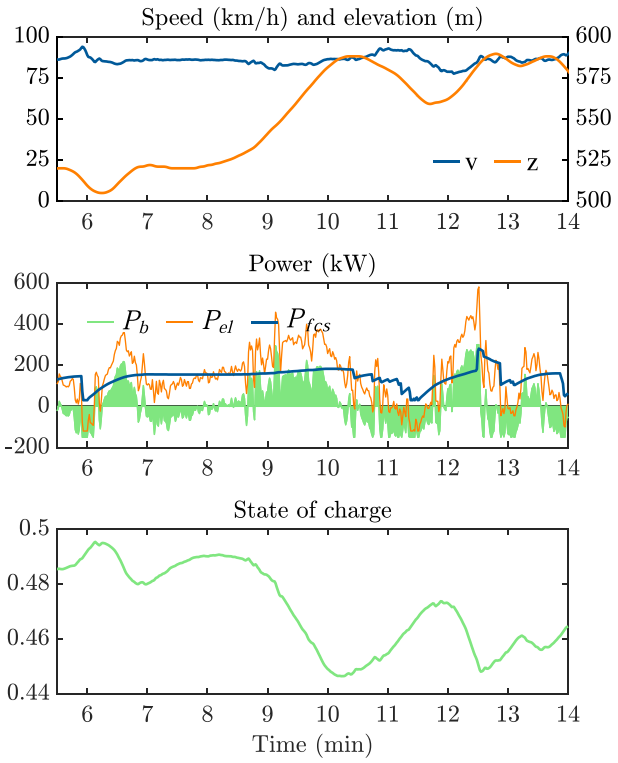

Fig. 11. Example of power-split using NLP for a fragment of driving cycle.

RPA) determine higher hydrogen consumption.

6.4. Analysis of robustness

The robustness of the proposed online energy management strategies is proved thoroughly in this work. Firstly, the robustness to unknown driving cycles is guaranteed by tuning the EMS parameters on a subset of cycles. Secondly, examining all the cycles in sequence, the strategies' effectiveness is retained, and the battery is never entirely charged nor discharged. However, to test the battery charge's robustness furtherly, each cycle is run starting with a highly depleted (10%) or charged (90%) battery. This analysis confirms that all strategies can re-establish regular operation without violating the battery's physical constraints (complete discharge and overcharge). Fig. 13 shows an example of the test for a single driving cycle using NLP.

6.5. Analysis of computational complexity

The strategies under investigation have different computational complexities. Table 5 compares the time required to simulate 1750 driving hours, considering all the cycles in sequence. In general, the simulation time is significantly lower than the driving time for all strategies. However, RB, NLP, and ECMS show a particularly low computational complexity. In this case, it is almost irrelevant that RB is about 20 times faster than NLP and ECMS. On the contrary, PMP requires more simulation time because of the iterations to converge to the state of charge target at the end of the cycle. MPC requires even higher simulation time because it involves receding horizon optimizations. The values reported in Table 5 refer to simulations performed using MATLAB R2020a on a computer with 1.80 GHz of base CPU speed and 16 Gb of RAM.

7. Conclusions

This paper investigates the design of energy management strategies for heavy-duty fuel cell vehicles considering an extensive and realistic

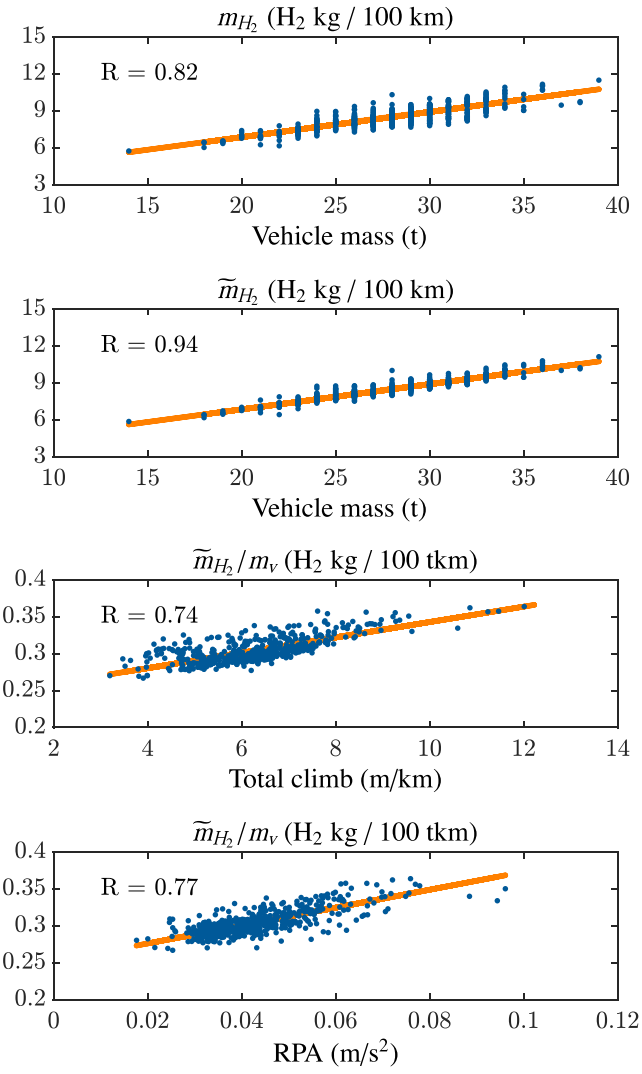

Fig. 12. Correlation between minimum hydrogen consumption and driving features (i.e. vehicle mass, total climb and RPA).

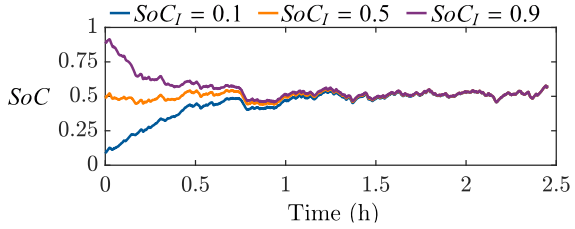

Fig. 13. Example of test to verify the robustness of strategies in terms of charge sustaining. The strategy under analysis is NLP.

Table 5
Computational time required to simulate 1750 driving hours.

Strategy	RB	NLP	ECMS	PMP	MPC
Comp. time (s)	4.7	99.5	111.0	1319.2	10961.3

representation of road freight transportations. The simulation results' analysis proves that energy management investigations should always examine numerous driving cycles to statistically validate control strategies and avoid significant misjudgments of the performance indexes.

This investigation also establishes that it is critical to consider real-world speed, elevation, and truck loading conditions because they determine high vehicle performance variations. In particular, a robust design of energy management strategies for heavy-duty vehicles cannot neglect road slope and truck loading conditions because they heavily affect the electric loads.

The strategies investigated in this work provide a broad and comprehensive understanding of the energy management of heavy-duty fuel cell vehicles. In particular, Pontryagin's minimum principle defines the benchmark for the hydrogen economy, finding its theoretical limits. However, ECMS can achieve the same results using only the available driving information. On the contrary, for the multi-objective optimization of the hydrogen economy and system lifetime, Pontryagin's minimum principle cannot be used as a benchmark because it is not sufficient for the global optimality. On the other hand, MPC determines a substantial reduction of the fuel cell transients while retaining a high hydrogen economy, highlighting the potential benefits of predictive energy management strategies. The results of RB and NLP are also significant in comparison to PMP_H. In these cases, the optimal tuning using evolutionary algorithms is excellent for the strategies' robustness and effectiveness, leading to the conclusion that even a simple heuristic strategy can achieve good results if properly tuned.

The limitations of this work indicate potential research directions for the advancement of energy management strategies for heavy-duty fuel cell vehicles. The study of predictive strategies requires further investigations to evaluate the drawbacks related to uncertain load predictions. Moreover, the strategies can develop to actively include the battery lifetime and the restraint of fuel cell high-power operation as additional targets. Eventually, as the optimization problem's complexity increases, dynamic programming could find the performance indexes' theoretical limits and define the benchmarks for online energy management strategies.

CRediT authorship contribution statement

Alessandro Ferrara: Conceptualization, Methodology, Software, Writing - original draft, Writing - review & editing, Visualization. **Stefan Jakubek:** Supervision, Project administration, Funding acquisition. **Christoph Hametner:** Conceptualization, Writing - review & editing, Supervision, Project administration, Funding acquisition.

Declaration of Competing Interest

The authors declare that they have no known competing financial interests or personal relationships that could have appeared to influence the work reported in this paper.

Acknowledgments

The financial support by the Austrian Federal Ministry for Digital and Economic Affairs and the National Foundation for Research, Technology and Development is gratefully acknowledged. This work has been created in cooperation with the Austrian research project "HyTruck" (Grant No. 868790).

Appendix A. Fuel cell degradation

In vehicle applications, fuel cell degradation is accelerated by frequent start-up/shut-down cycles, transient loads, low and high power operation. Therefore, lifetime expectations are typically shorter than stationary applications (e.g., 5000 h vs. 40000 h [6]). In particular, in a review of experimental techniques to measure degradation, Zhao and Li [7] identify average voltage degradation rates of 1 μV/h in stationary operation and 100 μV/h in transient operation.

Table A.6 summarizes fuel cell degradation phenomena from a review of the relevant literature [6–9]. Transient loads induce temperature/humidity changes, potential cycling, and reactant starvation. Temperature/humidity changes cause mechanical degradation of the membrane electrode assembly (MEA): shrinking-swelling cycles determine cracks, delamination, ionomer redistribution, and pinholes in the membrane. Potential cycling accelerates platinum particles' degradation on carbon supports due to Pt dissolution, migration, agglomeration, and Ostwald ripening. A basic explanation of these phenomena is offered in [39]. Reactant starvation can occur locally or on a larger scale. Local hydrogen starvation causes critical potentials in the cathode and consequent corrosion of the carbon support. Global hydrogen starvation causes abnormal reactions in the anode to provide protons and maintain the load current, determining carbon support corrosion. Air starvation determines a decrease in the cathode potential and formation of hydrogen due to abnormal reactions. Thus, hot spots generate from the direct reaction of hydrogen and oxygen, which is highly exothermic. Carbon corrosion and catalyst degradation determine permanent loss of electrochemically active area, higher charge, and mass transfer resistances.

During start-up, fuel cells experience the inevitable transition between air-filled and hydrogen-filled anodes. The opposite transition occurs during shut-down. Therefore, moving air/hydrogen boundaries are established during start-up/shut-down cycles. The anode potential decreases in the air-filled region, causing a higher difference with the cathode. Abnormal reactions corrode the cathode's carbon support and produce protons, which then move to the anode, generating the so-called reverse current. Additionally, cold starts and shut-downs cause severe structural damage within the MEA

Table A.6
Summary of the main fuel cell degradation phenomena: dynamic loads (DL); start/shutdown (SS); low power (LP); high power (HP).

Cause		Effect
Temperature/humidity change	$\xrightarrow{DL}$	Mechanical degradation
Reactant starvation	$\xrightarrow{DL}$	Carbon corrosion
Potential cycling	$\xrightarrow{DL}$	Catalyst degradation
Air/hydrogen boundary	$\xrightarrow{SS}$	Carbon corrosion
Sub-zero temperatures	$\xrightarrow{SS}$	Mechanical degradation
Reactant crossover	$\xrightarrow{LP}$	Chemical degradation
High temperatures	$\xrightarrow{HP}$	Membrane degradation

due to frost-heave and water volume expansion during freezing.

Low-power operations determine chemical degradation of the membrane due to intensified reactant crossover and high potentials. Indeed, direct reactions cause hotspots in the cathode and generate free radicals in the anode, which chemically attacks the membrane. Higher partial pressures due to limited reactions promote gas crossover. Low water generation leads to membrane dehydration, opening pores for gas permeation. Moreover, oxygen crossover is promoted by a lack of intense proton and water fluxes to the cathode. Details about water transport phenomena and membrane nanostructure can be found in [40].

High-power operations cause flooding in the cathode due to excessive water generation. However, on the anode side, the membrane is dehydrated due to high proton currents, which hinder water's back-flow. Therefore, without proper water and thermal management, the high-power operation can cause mechanical and chemical degradation of the membrane due to dehydration and high temperatures.

References

[1] Lee D-Y, Elgowainy A, Kotz A, Vijayagopal R, Marcinkoski J. Life-cycle implications of hydrogen fuel cell electric vehicle technology for medium- and heavy-duty trucks. J Power Sources 2018;393:217–29. https://doi.org/10.1016/j.jpowsour.2018.05.012.

[2] Mulholland E, Teter J, Cazzola P, McDonald Z, Gallachóir BPÓ. The long haul towards decarbonising road freight – a global assessment to 2050. Appl Energy 2018;216:678–93. https://doi.org/10.1016/j.apenergy.2018.01.058.

[3] Kast J, Vijayagopal R, Gangloff JJ, Marcinkoski J. Clean commercial transportation: medium and heavy duty fuel cell electric trucks. Int J Hydrogen Energy 2017;42(7):4508–17. https://doi.org/10.1016/j.ijhydene.2016.12.129.

[4] Liu F, Zhao F, Liu Z, Hao H. The impact of fuel cell vehicle deployment on road transport greenhouse gas emissions: the china case. Int J Hydrogen Energy 2018;43(50):22604–21. https://doi.org/10.1016/j.ijhydene.2018.10.088.

[5] Kast J, Morrison G, Gangloff JJ, Vijayagopal R, Marcinkoski J. Designing hydrogen fuel cell electric trucks in a diverse medium and heavy duty market. Res Transp Econ 2018;70:139–47. https://doi.org/10.1016/j.retrec.2017.07.006.

[6] Ren P, Pei P, Li Y, Wu Z, Chen D, Huang S. Degradation mechanisms of proton exchange membrane fuel cell under typical automotive operating conditions. Prog Energy Combust Sci 2020;80. https://doi.org/10.1016/j.pecs.2020.100859. 100859.

[7] Zhao J, Li X. A review of polymer electrolyte membrane fuel cell durability for vehicular applications: degradation modes and experimental techniques. Energy Convers Manage 2019;199. https://doi.org/10.1016/j.enconman.2019.112022. 112022.

[8] Borup R, Meyers J, Pivovar B, Kim YS, Mukundan R, Garland N, et al. Scientific aspects of polymer electrolyte fuel cell durability and degradation. Chem Rev 107 (10): 2007; 3904–3951. doi:10.1021/cr050182l. URL https://doi.org/10.1021/cr050182l.

[9] Pei P, Chang Q, Tang T. A quick evaluating method for automotive fuel cell lifetime. Int J Hydrogen Energy 2008;33(14):3829–36. https://doi.org/10.1016/j.ijhydene.2008.04.048.

[10] Guzzella L, Sciarretta A. Vehicle propulsion systems. Springer Berlin Heidelberg; 2013. doi:10.1007/978-3-642-35913-2. URL https://doi.org/10.1007/978-3-642-35913-2.

[11] Ferrara A, Okoli M, Jakubek S, Hametner C. Energy management of heavy-duty fuel cell electric vehicles: Model predictive control for fuel consumption and lifetime optimization. IFAC-PapersOnLine x(x): 2020; x–x. doi:10.1016/j.ifacol.2020.12.1053.

[12] Kemper P, Rehlaender P, Witkowski U, Schwung A. Competitive evaluation of energy management strategies for hybrid electric vehicle based on real world driving. In: 2017 European modelling symposium (EMS), IEEE; 2017. p. 151–156. doi: 10.1109/ems.2017.35. URL https://doi.org/10.1109/ems.2017.35.

[13] Ravey A, Blunier B, Miraoui A. Control strategies for fuel-cell-based hybrid electric vehicles: from offline to online and experimental results. IEEE Trans Vehic Technol 2012;61(6):2452–7. https://doi.org/10.1109/tvt.2012.2198680.

[14] Ettihir K, Boulon L, Agbossou K. Optimization-based energy management strategy for a fuel cell/battery hybrid power system. Appl Energy 2016;163:142–53. https://doi.org/10.1016/j.apenergy.2015.10.176.

[15] Fletcher T, Thring R, Watkinson M. An energy management strategy to concurrently optimise fuel consumption & PEM fuel cell lifetime in a hybrid vehicle. Int J Hydrogen Energy 2016;41(46):21503–15. https://doi.org/10.1016/j.ijhydene.2016.08.157.

[16] Zhou D, Ravey A, Al-Durra A, Gao F. A comparative study of extremum seeking methods applied to online energy management strategy of fuel cell hybrid electric vehicles. Energy Convers Manage 2017;151:778–90. https://doi.org/10.1016/j.enconman.2017.08.079.

[17] Song K, Chen H, Wen P, Zhang T, Zhang B, Zhang T. A comprehensive evaluation framework to evaluate energy management strategies of fuel cell electric vehicles. Electrochim Acta 2018;292:960–73. https://doi.org/10.1016/j.electacta.2018.09.166.

[18] Li X, Wang Y, Yang D, Chen Z. Adaptive energy management strategy for fuel cell/battery hybrid vehicles using pontryagin's minimal principle. J Power Sources 2019;440. https://doi.org/10.1016/j.jpowsour.2019.227105. 227105.

[19] Simmons K, Guezennec Y, Onori S. Modeling and energy management control design for a fuel cell hybrid passenger bus. J Power Sources 2014;246:736–46. https://doi.org/10.1016/j.jpowsour.2013.08.019.

[20] Geng C, Jin X, Zhang X. Simulation research on a novel control strategy for fuel cell extended-range vehicles. Int J Hydrogen Energy 2019;44(1):408–20. https://doi.org/10.1016/j.ijhydene.2018.04.038.

[21] Guo Q, Zhao Z, Shen P, Zhou P. Optimization management of hybrid energy source of fuel cell truck based on model predictive control using traffic light information. Control Theory Technol 2019;17(4):309–24. https://doi.org/10.1007/s11768-019-9118-1.

[22] Hu X, Zou C, Tang X, Liu T, Hu L. Cost-optimal energy management of hybrid electric vehicles using fuel cell/battery health-aware predictive control. IEEE Trans Power Electron 2020;35(1):382–92. https://doi.org/10.1109/tpel.2019.2915675.

[23] Wu J, Zhang N, Tan D, Chang J, Shi W. A robust online energy management strategy for fuel cell/battery hybrid electric vehicles. Int J Hydrogen Energy 2020;45(27):14093–107. https://doi.org/10.1016/j.ijhydene.2020.03.091.

[24] Hu Z, Li J, Xu L, Song Z, Fang C, Ouyang M, Dou G, Kou G. Multi-objective energy management optimization and parameter sizing for proton exchange membrane hybrid fuel cell vehicles. Energy Convers Manage 2016;129:108–21. https://doi.org/10.1016/j.enconman.2016.09.082.

[25] Liu C, Liu L. Optimal power source sizing of fuel cell hybrid vehicles based on pontryagin's minimum principle. Int J Hydrogen Energy 2015;40(26):8454–64. https://doi.org/10.1016/j.ijhydene.2015.04.112.

[26] Enang W, Bannister C. Modelling and control of hybrid electric vehicles (a comprehensive review). Renew Sustain Energy Rev 2017;74:1210–39. https://doi.org/10.1016/j.rser.2017.01.075.

[27] Pukrushpan JT, Peng H, Stefanopoulou AG. Control-oriented modeling and analysis for automotive fuel cell systems. J Dyn Syst Measure Control 2004;126(1):14–25. https://doi.org/10.1115/1.1648308.

[28] Fan L, Zhang G, Jiao K. Characteristics of PEMFC operating at high current density with low external humidification. Energy Convers Manage 2017;150:763–74. https://doi.org/10.1016/j.enconman.2017.08.034.

[29] Luna J, Usai E, Husar A, Serra M. Enhancing the efficiency and lifetime of a proton exchange membrane fuel cell using nonlinear model-predictive control with nonlinear observation. IEEE Trans Ind Electron 2017;64(8):6649–59. https://doi.org/10.1109/tie.2017.2682787.

[30] Wang B, Wu K, Yang Z, Jiao K. A quasi-2d transient model of proton exchange membrane fuel cell with anode recirculation. Energy Convers Manage 2018;171:1463–75. https://doi.org/10.1016/j.enconman.2018.06.091.

[31] Murschenhofer D, Kuzdas D, Braun S, Jakubek S. A real-time capable quasi-2d proton exchange membrane fuel cell model. Energy Convers Manage 2018;162:159–75. https://doi.org/10.1016/j.enconman.2018.02.028.

[32] Büchi FN, Freunberger SA, Reum M, Paganelli G, Tsukada A, Dietrich P, Delfino A. On the efficiency of an advanced automotive fuel cell system. Fuel Cells 2007;7(2):159–64. https://doi.org/10.1002/fuce.200500257.

[33] Braun A, Rid W. The influence of driving patterns on energy consumption in electric car driving and the role of regenerative braking. Transp Res Procedia 2017;22:174–82. https://doi.org/10.1016/j.trpro.2017.03.024.

[34] Onori S, Serrao L, Rizzoni G. Hybrid electric vehicles. Springer London; 2016. doi:10.1007/978-1-4471-6781-5. URL https://doi.org/10.1007/978-1-4471-6781-5.

[35] Serrao L, Onori S, Rizzoni G. A comparative analysis of energy management strategies for hybrid electric vehicles, Journal of Dynamic Systems, Measure Control 133 (3). doi:10.1115/1.4003267. doi: 10.1115/1.4003267.

[36] Zhou Y, Li H, Ravey A, Péra M-C. An integrated predictive energy management for light-duty range-extended plug-in fuel cell electric vehicle. J Power Sources 2020;451. https://doi.org/10.1016/j.jpowsour.2020.227780. 227780.

[37] MATLAB, Particle swarm optimization: documentation, Copyright 2012–2019 The MathWorks, Inc. https://mathworks.com/help/gads/particleswarm.html.

[38] Venkateswarlu C, Jujjavarapu SE. Stochastic and evolutionary optimization algorithms. In: Stochastic global optimization methods and applications to chemical, biochemical, pharmaceutical and environmental processes. Elsevier; 2020. p. 87–123. doi:10.1016/b978-0-12-817392-3.00004-1. doi: 10.1016/b978-0-12-817392-3.00004-1.

[39] Meier JC, Galeano C, Katsounaros I, Witte J, Bongard HJ, Topalov AA, Baldizzone C, Mezzavilla S, Schüth F, Mayrhofer KJJ. Design criteria for stable pt/c fuel cell catalysts. Beilstein J Nanotechnol 2014;5:44–67. https://doi.org/10.3762/bjnano.5.5.

[40] Ferrara A, Polverino P, Pianese C. Analytical calculation of electrolyte water content of a proton exchange membrane fuel cell for on-board modelling applications. J Power Sources 2018;390:197–207. https://doi.org/10.1016/j.jpowsour.2018.04.005.